Chemistry of Metals and Alloys

Chem. Met. Alloys 10 (2017) 99-105
Ivan Franko National University of Lviv
www.chemetal-journal.org

First-principles prediction of stable phases in the Mg–Rh–B–H system

V.I. IVASCHENKO[1], I.Yu. ZAVALIY[2]*, P.E.A. TURCHI[3], N.R. MEDUKH[1], Yu.V. VERBOVYTSKYY[2]

[1] *Institute for Problems of Materials Science, NAS of Ukraine, Krzhyzhanivskoho St. 3, 03142 Kyiv, Ukraine*
[2] *Physico-Mechanical Institute, NAS of Ukraine, Naukova St. 5, 79060 Lviv, Ukraine*
[3] *Lawrence Livermore National Laboratory (L-352), P.O. Box 808, Livermore, CA 94551, USA*
* *Corresponding author. Tel.:* +380-32-2296833*; e-mail: zavaliy@ipm.lviv.ua*

Received October 7, 2017; accepted December 27, 2017; available on-line April 1, 2018

A first-principles investigation of plausible structures of the Mg–Rh–B–H system was carried out. The initial crystal structures of the Mg–Rh–B–H phases obtained by filling the voids in the Ti_2Ni structure type by boron or/and hydrogen atoms, were subsequently optimized. The optimum crystal structures were determined on the basis of an analysis of formation energies and densities of electronic states. The stable phases were predicted to be those in which the boron atoms form $B@Rh_4$ units, and the hydrogen atoms form $H@RhMg_3$ and $H@Rh_4$ units. Plausible origins of the stability of the Mg–Rh–B–H structures are discussed.

First-principles calculations / Crystal structure / Electronic state / Intermetallics / Hydride

1. Introduction

Mg–Rh–H phases with the Ti_2Ni structure type are stabilized by hydrogen incorporation [1]. Neutron diffraction has revealed that the hydrogen and deuterium atoms mainly occupy tetrahedral interstitial voids, whereas the octahedral voids are much less occupied. Alekseeva *et al.* [2] described the preparation and chemical bonding of the new ternary magnesium-rhodium-boron compound Mg_8Rh_4B, the first representative of the Ti_2Ni structure in which boron atoms occupy tetrahedral voids. To our knowledge, first-principles investigations of possible stable phases with the Ti_2Ni structure type with different extents of occupancy of the tetrahedral and octahedral voids have not yet been carried out. Such investigations are supposed to help scientists to synthesize new materials based on the Mg–Rh–B–H system for the storage of hydrogen and other applications.

In this work the results of first-principles calculations of various phases based on the Mg–Rh–B–H system are reported. Several stable phases are predicted and some of them have been confirmed experimentally. The paper is organized as follows: In section 2 details of the computations are described; section 3 contains the results of the first-principles calculations and their discussion; in section 4, the main conclusions are summarized.

2. Computational method used

As mentioned above, in our investigations we focused on the cubic structures of the Mg–Rh–B–H system based on the Ti_2Ni structure type (space group *Fd*-3*m*) with 96 metallic atoms in the unit cell. Hydrogen or other non-metal atoms can be located in 64 interstices per cell. Consequently, the investigated structure contains 160 atoms within the unit cell, provided that all voids are filled by boron or hydrogen atoms. We transformed the large face-centered cubic cell to the primitive rhombohedral cell. This transformation allowed us to reduce the computation time significantly, without losing the accuracy of the calculations.

Tables 1 and 2 show the atomic coordinates referring to the cubic 160-atom cell and to the rhombohedral 40-atom cell, respectively. The latter unit cell is shown in Fig. 1. The rhombohedral structures of different phases were obtained from the $Mg_{16}Rh_8H0_2H1_4H2_8H3_2$ structure (H0, H1, H2 and H3 are hydrogen (boron) atoms, *cf.* Table 1) by removing different non-metal atoms.

To validate such an approach we calculated the total energies (E_T) of the cubic $Mg_{64}Rh_{32}B_8$ and trigonal $Mg_{16}Rh_8B_2$ structures. The values of E_T of the two presentations were found to differ by 0.0007 eV/atom. This means that the structures are effectively equivalent.

The Ti_2Ni structure (cubic cell with *Fd*-3*m* space group) can according to the International Tables for Crystallography be described using two different origins. For the experimentally determined structure of $Mg_8Rh_4BD_{3+x}$, which is described in another paper of this issue, origin choice 1 was used. The trigonal version with the origin at an inversion center (origin choice 2) was used for the calculations in this paper. For comparison, the relation between the two origin choices of the cubic unit cell and the description in the primitive rhombohedral cell used in this paper are shown in Fig. 2.

The present calculations were done using the first-principles pseudopotential DFT method as implemented in the quantum ESPRESSO code [3] with periodic boundary conditions. The generalized gradient approximation (GGA) of Perdew, Burke and Ernzerhof [4] was used for the exchange-correlation energy and potential, and Vanderbilt ultra-soft pseudo-potentials were used to describe the electron-ion interaction [5]. In this approach, the orbitals are allowed to be as soft as possible in the core regions, so that their plane-wave expansion converges rapidly [5]. Non-linear core corrections were taken into account as described in [3]. The criterion of convergence for the total energy was 10^{-6} Ry/cell ($1.36 \cdot 10^{-5}$ eV/cell).

The initial structures were optimized by simultaneously relaxing the atomic basis vectors and the positions of the atoms inside the unit cell |using the Broyden-Fletcher-Goldfarb-Shanno (BFGS) algorithm [6]. The relaxation of the atomic coordinates and unit cell was considered to be complete when the atomic forces were less than 1.0 mRy/a_0 (25.7 meV/Å), the stresses were smaller than 0.05 GPa, and the total energy during the iterative structural optimization process was changing by less than 0.1 mRy/cell (1.36 meV/cell). The cut-off energy for the plane-wave basis E_{cut} was 36 Ry (490 eV). To speed up the convergence, each eigenvalue was convoluted with a Gaussian of a width of $\sigma = 0.025$ Ry (0.34 eV). The Monkhorst-Pack (M-P) [7] (4 4 4) and (2 2 2) meshes were used for the trigonal and cubic large-scale structures of the Mg–Rh–B–H system. The (8 8 8) M-P mesh was used in the calculations for Rh and B. The calculations for H_2 and Mg_2Rh were carried out using the (4 4 4) M-P mesh. Finally, hexagonal Mg was calculated using the (8 8 6) M-P mesh. The densities of states (DOS) were calculated using the tetrahedron method implemented in the computational code [3]. The cell transformations were performed using the PCW [8] and ISOTROPY [9] codes.

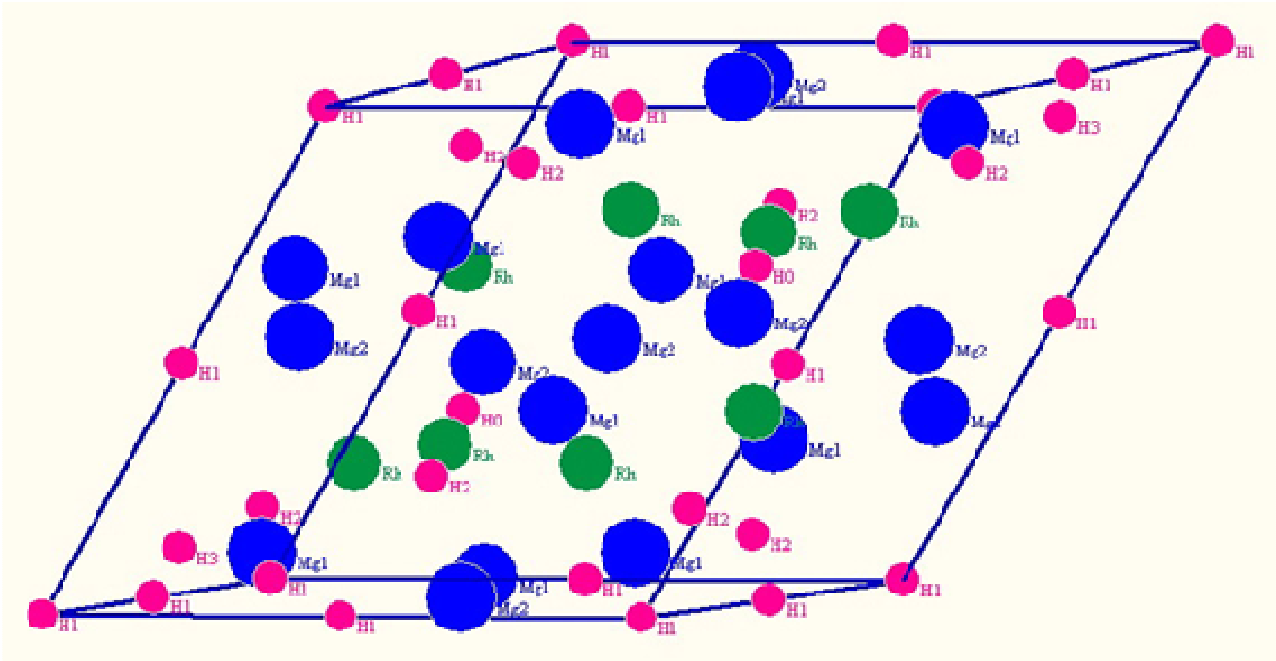

Fig. 1 Reduced rhombohedral cell for $Mg_{16}Rh_8H0_2H1_4H2_8H3_2$ (40 atoms, *R*-3*m*, No. 166), which reproduces the cubic structure of $Mg_{64}Rh_{32}H0_8H1_{16}H2_{32}H3_8$ (160 atoms, *Fd*-3*m*, No. 227). The large blue circles, medium green circles and small red circles represent the Mg, Rh and H (B) atoms, respectively.

Table 1 Atomic coordinates for $Mg_{64}Rh_{32}H0_8H1_{16}H2_{32}H3_8$ referring to the conventional cubic cell (a = 12.171 Å, *Fd*-3*m*, No. 227).

Atom	Wyckoff position	*x/a*	*y/b*	*z/c*	Surrounding of the H-atoms
Mg1	48*f*	0.199	0.000	0.000	–
Mg2	16*d*	0.625	0.625	0.625	–
Rh	32*e*	0.405	0.405	0.405	–
H0	8*b*	0.500	0.500	0.500	$H0\text{-}Rh_4$
H1	16*c*	0.125	0.125	0.125	$H1\text{-}Mg_6$
H2	32*e*	0.925	0.925	0.925	$H2\text{-}Mg_3Rh$
H3	8*a*	0.000	0.000	0.000	$H3\text{-}Mg_6$

Table 2 Atomic coordinates for $Mg_{16}Rh_8H0_2H1_4H2_8H3_2$ referring to the primitive rhombohedral cell (a = 8.6062 Å, *R*-3*m*, No. 166).

Atom	Wyckoff position	*x/a*	*y/b*	*z/c*
Mg1	6*h*	0.324	0.324	0.324
Mg1	6*h*	0.926	0.926	0.324
Mg2	1*b*	0.500	0.500	0.500
Mg2	3*e*	0.000	0.500	0.500
Rh	2*c*	0.720	0.720	0.720
Rh	6*h*	0.720	0.720	0.340
H0	2*c*	0.625	0.625	0.625
H1	1*a*	0.000	0.000	0.000
H1	3*d*	0.500	0.000	0.000
H2	2*c*	0.200	0.200	0.200
H2	6*h*	0.200	0.200	0.900
H3	2*c*	0.125	0.125	0.125

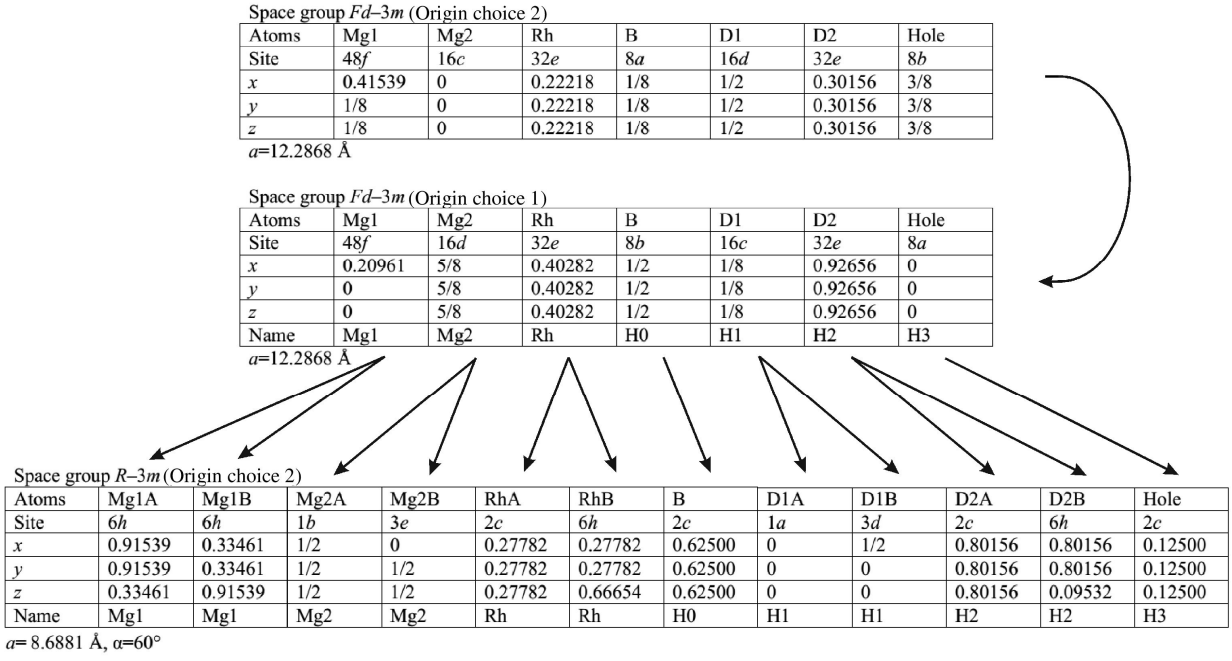

Fig. 2 Relation between the two origin choices of the cubic unit cell (space group *Fd*-3*m*) and the description in the primitive rhombohedral cell (*R*-3*m*).

The formation energies of the bulk materials were calculated as $E = E_{tot} - \sum n_i E_i$, where E_{tot} is the total energy of the structures of the Mg–Rh–B–H system with n_i atoms of the element i (Mg, Rh, B, and H) and E_i is the total energy of bulk Mg, Rh, B and half of the energy of an H_2 molecule. The following formation energies were considered:

$$E1 = E_{tot}(Mg_{16}Rh_8H0_2H1_4H2_8H3_2) - 16 \times E_{tot}(Mg) - 8 \times E_{tot}(Rh) - 16 \times 1/2 \times E_{tot}(H_2); \quad (1)$$

$$E2 = E_{tot}(Mg_{16}Rh_8H0_2H1_4H2_8H3_2) - 4 \times E_{tot}(Mg_4Rh_2) - 16 \times 1/2 \times E_{tot}(H_2), \text{ or}$$

$$E2 = E1(Mg_{16}Rh_8H0_2H1_4H2_8H3_2) - 24/N_a \times E1(Mg_4Rh_2); \quad (2)$$

$$E3 = E_{tot}(Mg_{16}Rh_8H0_2H1_4H2_8H3_2) - E_{tot}(Mg_{16}Rh_8H0_2) - 14 \times 1/2 \times E_{tot}(H_2), \text{ or}$$

$$E3 = E1(Mg_{16}Rh_8H0_2H1_4H2_8H3_2) - 26/N_a \times E1(Mg_{16}Rh_8H0_2); \quad (3)$$

$$E3' = E1(Mg_{16}Rh_8B0_2H1_4H2_8H3_2) - 26/N_a \times E1(Mg_{16}Rh_8B0_2), \quad (4)$$

where N_a is the number of atoms in the cell. These expressions are also valid for borides. In this case, the hydrogen atoms are replaced by boron atoms and $1/2E_{tot}(H_2)$ should be replaced by $E_{tot}(B)$. The conditions for the calculations for Mg, Rh and B were described above. We calculated the total energy and equilibrium bond length of the H_2 molecule using the extended two-atom cubic cell. The computed bond length of the H_2 molecule of 0.752 Å is in agreement with the experimental value of 0.740 Å [10] within 1.6%. The expression 1 implies that the materials are synthesized from Mg, Rh and H_2 or/and B. The tetragonal Mg_4Rh_2 phase and H_2 or/and B are needed to synthesize the materials according to the expression 2. Finally, the expressions 3 and 4 indicate the path for synthesizing the materials using $Mg_{16}Rh_8H0_2$ and $Mg_{16}Rh_8B0_2$, respectively, as main precursors.

To estimate the formation energies of the Mg–Rh–B–H structures we first calculated the total energies of Mg, Rh, B, H_2, Mg_2Rh, $Mg_{16}Rh_8$, and $Mg_{16}Rh_8B_2$. The results are summarized in Table 3. One can see that the calculated structural parameters are very close to those found experimentally.

3. Results and discussion

Table 4 shows the formation energies of different phases of the trigonal (cubic) Mg–Rh–B–H phases described in Tables 1 and 2 and Fig. 1. It should be kept in mind that the lower the formation energy, the higher the stability of the material, and that a material can be synthesized provided that its formation energy is negative. For the majority of the structures the values of $E1$ are negative. This means that these structures can be prepared from the elements Mg, Rh, B and H. A comparison of the energies $E1$ and $E2$ shows that the formation energies of Mg_4Rh_2 and $Mg_{16}Rh_8B0_2$ are comparable and larger than those of the other structures. It follows that, during the synthesis of each structure, first the Mg_4Rh_2 and $Mg_{16}Rh_8B0_2$ compounds will be formed. Hence, to estimate the stability of the phases presented in Table 4, first of all we should take into account the values of $E2$ and $E3$. Following this rule, we singled out the most stable structures, which are shaded in Table 4.

Table 3 Structural and energetic parameters of the Mg–Rh–B–H phases considered in this investigation. N_a – number of atoms in the unit cell, a, b, c – basis vectors of the unit cell, E_T – total energy, $E1$, $E2$, $E3$ – formation energies. Notations of the structures used in this paper are given in braces; experimental values are given in parentheses.

Phase	Space group	N_a	a (Å)	b (Å)	c (Å)	E_T (eV/atom)	$E1$, $E2$ (eV/atom)
Mg	$P6_3/mmc$	2	3.221 (3.209)[a]	3.221 (3.209)[a]	5.183 (5.210)[a]	-1920.6845	–
Rh	Fm-3m	1	3.878 (3.830)[b]	–	–	-601.6028	–
B	R-3m	12 36	5.041 4.893 (4.908)[c]	5.041 4.893 (4.908)[c]	5.041 12.524 (12.567)[c]	-84.0750	–
H_2	Pm-3m	2	5.000[d]	–	–	-15.8454	–
$Mg_{16}Rh_8$ $Mg_{64}Rh_{32}$	R-3m Fd-3m	24 96	8.477 11.988	8.477 11.988	8.477 11.988	-1481.4285	$E1$ = -0.428
Mg_4Rh_2 {t-MR}	$I4/mmm$	6	3.213 (3.188)[e]	3.213 (3.188)[e]	10.142 (10.066)[e]	-1481.4417	$E1$ = -0.451
$Mg_{16}Rh_8B_2$ {MRB0}	R-3m Fd-3m	26 104	8.667 12.256 (12.171)[f]	8.667 12.256 (12.171)[f]	8.667 12.256 (12.171)[f]	-1373.9976	$E1$ = -0.462 $E2$ = -0.046

[a] PDF file [089-4037]; [b] PDF file [088-2334]; [c] PDF file [012-0377]; [d] the simple cubic unit cell with two hydrogen atoms was used to determine the total energy of the H_2 molecule, the equilibrium bond length 0.752 Å is close to the experimental value of 0.741 Å [10]; [e] [1]; [f] [2].

Some of these structures have been observed experimentally, and $Mg_{16}Rh_8H0_2$ (MRH0), $Mg_{16}Rh_8H2_8$ (MRH2), $Mg_{16}Rh_8H0_2H2_8$ (MRH0H2) are predicted to be quite stable. The $Mg_{16}Rh_8B0_2H2_8$ (MRB0H2) and $Mg_{16}Rh_8B0_2H1_4H2_8$ (MRB0H1H2) phases are predicted to be the most stable hydrides of the Mg_8Rh_4B compound. This prediction was confirmed by the experimentally determined structure of the $Mg_8Rh_4BD_{3+x}$ deuteride (see other paper in this issue). The negative $E3$ energy (Table 4) is an evidence of the coincidence of the experimental and calculated models, even taking into account that full occupation of positions H1 and H2 were used for the theoretical calculations.

Let us analyze the stability of the phases under consideration in terms of chemical bonding. To do this we need information on the local partial densities of states (PDOS). The PDOS of the most stable basic t-MR and MRB0 phases are shown in Figs. 3 and 4. For t-MR, there is a narrow band below the Fermi level (E_F) in the DOS. This band originates from Rh *d*-states, and consists of t_{2g} and e_g states. The e_g-states are localized at the center of the Rh *d*-band, whereas the t_{2g}-states form the DOS peak just below E_F. The Mg *s*- and *p*-states are distributed over all the bands and mainly form the DOS at the Fermi level.

In the electronic spectrum of MRB0 we singled out several bands marked with Roman numerals (*cf.* Fig. 4). The band I is mostly composed of B 2*s*-states and contains an admixture of Rh *d*- and Mg *p*-states. The boron 2*p*-states make the main contribution to the band II. In this region, Rh *d*-states are also present, for which reason the band II can be designated as the bonding B *p*-Rh *d* band.

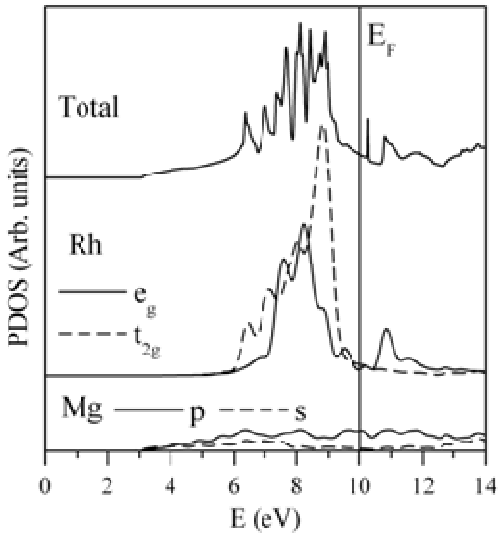

Fig. 3 Local partial density of states (PDOS) for t-MR. Here and in further figures, the vertical line denotes the Fermi level.

Table 4 Total energy (E_T) and formation energies ($E1$, $E2$, $E3$, $E3'$) for different structures of the Mg–Rh–B–H system. Denotation of the elements in the structural formula: M – Mg (16 atoms per cell), R – Rh (8 atoms), B0 (H0) (2 atoms), B1 (H1) (4 atoms), B2 (H2) (8 atoms), B3 (H3) (2 atoms), as described in Tables 1 and 2. N_a is the number of atoms in the primitive rhombohedral cell. The most stable configurations are highlighted.

Structure	N_a	E_T (eV/atom)	$E1$ (eV/atom)	$E2$ (eV/atom)	$E3$, $E3'$ (eV/atom)
MRB0 [a]	26	-1373.9976	-0.462	-0.046	-
MRB1	28	-1281.4490	-0.018	+0.369	-
MRB2	32	-1132.035	-0.274	+0.065	-
MRB3	26	-1373.7750	-0.239	+0.177	-
MRB0B1B2B3	40	-921.9900	+0.234	+0.505	+0.534
MRH0	26	-1368.7214	-0.434	-0.018	-
MRH1	28	-1271.9766	-0.293	+0.114	-
MRH2	32	-1115.1417	-0.437	-0.099	-
MRH3	26	-1368.6357	-0.409	+0.008	-
MRH0H2	34	-1050.4871	-0.422	-0.103	-0.090
MRH0H1H2H3[a]	40	-895.2447	-0.312	-0.042	-0.030
MRB0H1	30	-1192.8462	-0.336	+0.024	+0.064
MRB0H2	34	-1054.4998	-0.421	-0.102	-0.068
MRB0H3	28	-1276.9434	-0.386	+0.001	+0.043
MRB0H1H2[a]	38	-945.1536	-0.362	-0.077	-0.046
MRB0H1H3	32	-1119.2757	-0.307	+0.031	+0.068
MRB0H2H3	36	-996.7065	-0.307	-0.006	+0.027
MRB0H1H2H3	40	-898.6041	-0.260	+0.011	+0.040

[a] Structures observed experimentally [1,2].

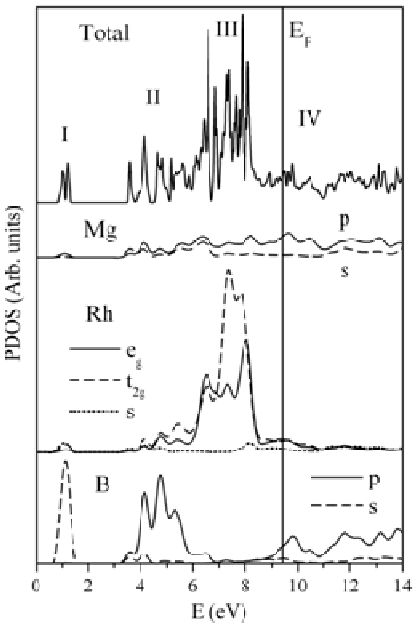

Fig. 4 Local partial densities of states (PDOS) for MRB0.

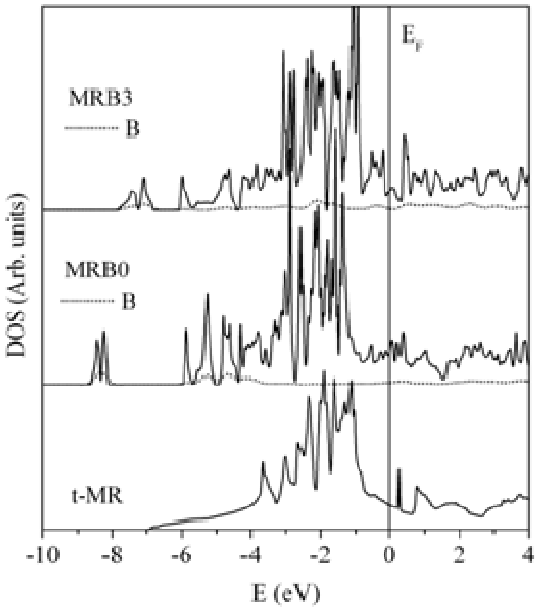

Fig. 5 Total densities of states (DOS) for t-MR, MRB0 and MRB3. The dotted lines indicate the local partial DOS of the boron atoms.

The band III consists of Rh *d*-states. As compared to t-MR, in MBRB0, the t_{2g} peak shifts towards lower energies owing to strong Rh–B–Rh interactions. Finally, in the band IV, the anti-bonding B 2*p*-Rh *d* states are localized. As in the case of t-MR, in MRB0 the Mg *s*- and *p*-states are present in small amounts in all the bands. Thus, the introduction of boron atoms into the H0 interstices (*cf.* Table 1) leads to the formation of B@Rh_4 units with strong covalent B-Rh bonds.

Fig. 4 shows the densities of states for the t-MR, MRB0 and MRB3 structures. As compared to MRB0, in MRB3, the B-Rh bands shift towards high energies. Besides, the B 2*p*-Rh *d* hybridized states are localized within the band III (*cf.* Figs. 4 and 5). The negative charges localized on the boron ions in MRB0 and MRB3 are -0.28e and -0.60e, respectively. These findings indicate that the B-Rh bonds in MRB3 are less covalent and more ionic than in MRB0. This change in chemical bonding is caused by the different surroundings of the boron atoms in the structures: B@Rh_4 in MRB0 and B@Mg_6 in MRB3 (*cf.* Table 1). It follows that, among the borides considered here, the structures in which the B atoms are surrounded by Rh atoms should be more stable (*e.g.* MRB0 and MRB2, *cf.* Tables 1 and 3).

We analyzed the local partial densities of states of the Mg–Rh–B–H phases to gain insight into the origin of the stability of these hydride phases. The PDOS of these structures are shown in Fig. 6. A comparison of the chemical bonding in the stable MRB0H2 and unstable MRB0H1 compounds shows that the hydrogen bands in MRB0H2 are lower than in MRB0H1. The excess charges concentrated on a hydrogen ion are -0.12e and -0.19e in MRB0H2 and MRB0H1, respectively.

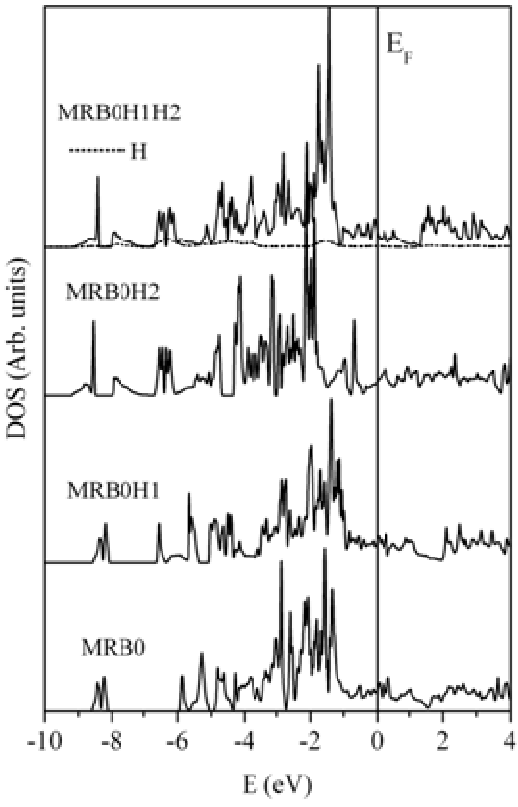

Fig. 6 Total densities of states (DOS) for MRB0, MRB0H1, MRB0H2, and MRB0H1H2. The dotted lines indicate the local partial DOS of the hydrogen atoms.

These results indicate that the H-Rh and H-Mg bonds in MRB0H2 are stronger than in MRB0H1. It follows that, for the hydrides, the main hydrogen configuration that determines the stability of these materials is the H-Mg_3Rh configuration, *i.e.* when the H atoms occupy H2 interstices (*cf.* Tables 1 and 3). An analysis of the PDOS of the Mg–Rh–H materials (not presented here) showed that the main features of the chemical bonding for the Mg–Rh–B–H compounds are inherent also to the Mg–Rh–H hydrides.

4. Conclusions

First-principles calculations of some structures of the Mg–Rh–B–H system based on the Ti_2Ni structure type were carried out to investigate their phase stability and chemical bonding. The initial structures that contained up to 140 atoms in the cubic cell, were described in the reduced 40-atom rhombohedral cells to facilitate the investigation of their stability. The formation energies, local partial densities of states and partial charges of the optimized Mg–Rh–B–H structures were calculated and analyzed. Some of the predicted stable structures have been observed experimentally, and other phases ($Mg_{16}Rh_8H0_2$, $Mg_{16}Rh_8H2_8$, $Mg_{16}Rh_8H0_2H2_8$, and $Mg_{16}Rh_8B0_2H2_8$) are predicted to be quite stable and may be synthesized in the future. The most stable compounds were found to be those in which the boron atoms form $B@Rh_4$ units, and the hydrogen atoms form $B@RhMg_3$ and $B@Rh_4$ units.

Acknowledgements

This investigation was supported by the Contract III-9-15 of the National Academy of Sciences of Ukraine. The work of P.E.A. Turchi was performed under the auspices of the U.S. Department of Energy by the Lawrence Livermore National Laboratory under contract No. DE-AC52-07NA27344.

References

[1] F. Bonhomme, P. Selvam, M. Yoshida, K. Yvon, *J. Alloys Compd.* 178 (1992) 167-172.
[2] A.M. Alekseeva, A.M. Abakumov, A. Leithe-Jasper, W. Schnelle, Yu. Prots, P.S. Chizhov, G. Van Tendeloo, E.V. Antipov, Yu. Grin, *J. Solid State Chem.* 179 (2006) 2751-2760.
[3] P. Giannozzi, S. Baroni, N. Bonini, M. Calandra, R. Car, C. Cavazzoni, D. Ceresoli, G.L. Chiarotti, M. Cococcioni, I. Dabo, A. Dal Corso, S. de Gironcoli, S. Fabris, G. Fratesi, R. Gebauer, U. Gerstmann, C. Gougoussis, A. Kokalj, M. Lazzeri, L. Martin-Samos, N. Marzari, F. Mauri, R. Mazzarello, S. Paolini, A. Pasquarello, L. Paulatto, C. Sbraccia, S. Scandolo, G. Sclauzero, A.P. Seitsonen, A. Smogunov, P. Umari, R.M. Wentzcovitch, *J. Phys: Condens. Matter* 21 (2009) 395502-19.
[4] J.P. Perdew, K. Burke, M. Ernzerhof, *Phys. Rev. Lett.* 77 (1996) 3865-3868.
[5] D. Vanderbilt, *Phys. Rev. B* 41 (1990) 7892-7895.
[6] S.R. Billeter, A. Curioni, W. Andreoni, *Comput. Mater. Sci.* 27 (2003) 437-445.
[7] H.J. Monkhorst, J.D. Pack, *Phys. Rev. B* 13 (1976) 5188-5192.
[8] W. Kraus, G. Nolze, *PowderCell for Windows (Version 2.4)*, Federal Institute for Research and Testing, Berlin, Germany, 2000.
[9] H.T. Stokes, D.M. Hatch, B.J. Campbell, *ISOTROPY*, 2007; http://stokes.byu.edu/isotropy.html
[10] H.H. Hyman, C.R. Seppesen, *Nature* 125 (1930) 462-462.